Available online at www.sciencedirect.com

ScienceDirect

Ceramics International 40 (2014) 943–950

CERAMICS INTERNATIONAL

www.elsevier.com/locate/ceramint

# ZnO nanoswords and nanopills: Hydrothermal synthesis, characterization and optical properties

A. Moulahi[a], F. Sediri[a,b,*]

[a]Laboratory of Condensed Matter Chemistry, IPEIT, University of Tunis, 2, Jawaher Lel Nehru 1008, B.P. 229 Montfleury, Tunisia
[b]Chemistry Department, Sciences Faculty of Tunis, Tunis El Manar University, 2092 El Manar, Tunisia

Received 10 June 2013; received in revised form 22 June 2013; accepted 24 June 2013
Available online 2 July 2013

**Abstract**

Nanostructured hexagonal zinc oxide pills and swords-like were hydrothermally synthesized using zinc sulfate heptahydrate ($ZnSO_4 \cdot 7H_2O$) as an inorganic precursor and adipic acid ($HOOC(CH_2)_4COOH$) as a structure-directing agent. The structure, the crystallinity, the morphology and the composition of the materials were investigated by X-ray diffraction (XRD), scanning electron microscopy (SEM), Fourier transform infrared spectroscopy (FTIR), Raman spectroscopy and X-ray photoelectron spectroscopy (XPS). XRD study demonstrated the existence of wrutzite ZnO of high degree of crystallinity with crystallite size in the range of 70–80 nm. The optical properties of the as-synthesized ZnO were investigated by UV–visible absorption and room temperature photoluminescence (RTPL). The band gap for ZnO nanswords and nanopills was found to be 3.25 and 3.27 eV, respectively.


*Keywords:* C. Optical properties; D. ZnO; Nanostructures; Hydrothermal synthesis

## 1. Introduction

Zinc oxide (ZnO) has attracted much attention for nanoscale electronic and optoelectronic device applications because of its wide band gap (3.37 eV) and large exciton binding energy (60 meV) [1]. It is also a well-known fact that ZnO is a polar crystal with hexagonal phase, and the high anisotropy of ZnO leads to the oriented growth along the *c* axis [2]. In terms of band energy, ZnO is a suitable alternative to $TiO_2$ [3]. Zinc oxide has been used in numerous applications, such as transparent electrodes in solar cells [4], light emitting diodes [5], gas sensors [6], acousto-optical devices [7], lasers [8], photocatalysis [9], antibacterial agents [10] and piezoelectric devices [11]. ZnO has been the focus of numerous research studies due to its low toxicity and low price, high chemical and thermal stability, high transparency in the visible wavelength range and unique optical properties. In its powder form, ZnO is a very important material for its potential applications in numerous areas such as electronics and photonics. ZnO nanoparticles are good candidates as inter-electrodes because of their superior optical properties (transparency in the visible spectral region) as well as their process capability based conventional solution processes [12].

Nanostructured ZnO has been synthesized using a variety of methods, as well as vapor-phase transport [13], chemical vapor deposition [14], magnetron sputtering [15], laser ablation [16], and wet chemical methods [17]. More recently, improved optimized routes, simple solution and hydrothermal treatment, for fabrication of nanostructured products have been also reported [18]. It is noticed that morphology of the synthesized nanostructures strongly depends on the synthesis route and the structure directing agents [19–21]. Hydrothermal synthesis, as an important method of wet chemistry, has attracted growing attention from scientists in general and chemists in particular; for its operational simplicity, low cost, high efficiency, as well as the possibility of its environmentally-safe large-scale production [22,23].

This paper deals with the synthesis of ZnO nanoswords and nanopills by hydrothermal reaction of zinc sulfate heptahydrate ($ZnSO_4 \cdot 7H_2O$) as an inorganic precursor and adipic acid

*Corresponding author at: Chemistry Department, Sciences Faculty of Tunis, Tunis El Manar University, 2092 El Manar, Tunisia. Tel.: +216 713 3664; fax: +216 7133 7323.
*E-mail addresses:* faouzi.sediri@ipeit.rnu.tn, sediri68@gmail.com (F. Sediri).

0272-8842/$ - see front matter © 2013 Elsevier Ltd and Techna Group S.r.l. All rights reserved.
http://dx.doi.org/10.1016/j.ceramint.2013.06.090

($HOOC(CH_2)_4COOH$) which acts as structure-directing, size and morphology-controlling agent. The impact of the reaction time on the particles size and the morphology was investigated. Although many methods have been developed to elaborate nanostructured zinc oxide ZnO, to the best of our knowledge, this is the first report of ZnO nanostructured synthesis using $ZnSO_4 \cdot 7H_2O$ and $HOOC(CH_2)_4COOH$ as a structure-directing template.

## 2. Experimental details

### 2.1. Hydrothermal synthesis

The material was prepared from $ZnSO_4 \cdot 7H_2O$ (0.196 g), $HOOC(CH_2)_4COOH$ (0.100 g), NaOH (0.273 g) and distilled water (5 mL) in the molar ratio $ZnSO_4 \cdot 7H_2O$:$HOOC(CH_2)_4COOH$=1. Once introduced in the above-mentioned order, reactants were stirred for few minutes. This done, the resulting suspension was introduced in an autoclave lined with Teflon steel for 4 h at 180 °C. The resulting white powder was washed with water and acetone to remove the residues of $HOOC(CH_2)_4COOH$. It was then left to dry for four hours at 80 °C. The pH of the solution remains close to pH≈12 during the whole synthesis. To investigate the formation process of ZnO nanocrystalline, time dependent experiments were carried out at 180 °C.

### 2.2. Characterization techniques

The X-ray powder diffraction data (XRD) patterns of all samples were recorded on a X'Pert Pro Panalytical diffractometer with CuKα radiation ($\lambda$=1.54056 Å) and graphite monochromator. The XRD measurements were carried out by applying a step scanning method ($2\theta$ range from 2° to 70°), the scanning rate is 0.03° $s^{-1}$ and the step time is 3 s. Solid samples were coated with gold in a Balzers Union SCD 40 sputter-coater and studied by Scanning Electron Microscopy (SEM) with a Cambridge Stereoscan 120 instrument at an accelerating voltage of 10 kV. Fourier-transform infrared spectra (FTIR) were recorded from 4000 to 400 $cm^{-1}$ on a Nicolet 380 spectrometer in pellets of samples dispersed in KBr. Raman spectroscopy was performed using a Jobin Yvon T 64000 spectrometer (blue laser excitation with 488 nm wavelength and < 55 mW power at the sample). X-ray photoelectron spectroscopy (XPS) experiments were performed using a Shimadzu ESCALAB, at room temperature. UV–visible spectra were performed on a Perkin Elmer UV–vis spectrophotometer. Photoluminescence (PL) spectroscopy was performed to investigate the optical properties of the samples using a 250 mm Jobin Yvon luminescence spectrometer.

## 3. Results and discussion

### 3.1. X-ray diffraction

Powder X-ray diffraction patterns of the mixture before hydrothermal treatment and the resulting samples synthesized at 180 °C for different reaction times (0.5, 1, 3 and 24 h) are shown in Fig. 1. As indicated, all of diffraction peaks can be perfectly indexed to the pure hexagonal wurtzite structured ZnO (space group $P_3^6mc$) with lattice constants of $a=b=3.25$ Å and $c=5.25$ Å which match with the reported data (JCPDS no. 36-1451). All peaks appear at $2\theta$=31.823, 34.476, 36.305, 47.595, 56.638, 62.906, 66.411, 68.002 and 69.299, corresponding to (100), (002), (101), (102), (110), (103), (200), (112) and (201), respectively. The results indicate that the products consist of pure phase and no characteristic peaks can be found from other phases or impurities. Additionally, the sharp and the small values of the full widths at half maxima (FWHM) of the XRD peaks reveal that the as-synthesized materials are of high purity and good crystallinity. It is well known that the growth rate of the different planes family follows the sequence (001) > (101) > (100) [24,25].

The average crystallite size of the as-synthesized materials was calculated by using Scherrer's formula:

$$L = \frac{0.89\,\lambda}{\beta\,\cos\theta}$$

where $L$ is the average crystallite size, $\lambda$=0.154056 nm, $\beta$ is the half maximum peak width and $\theta$ is the diffraction angle in degrees [26]. The average crystallite size values, calculated from XRD patterns of the samples synthesized for 0.5 and

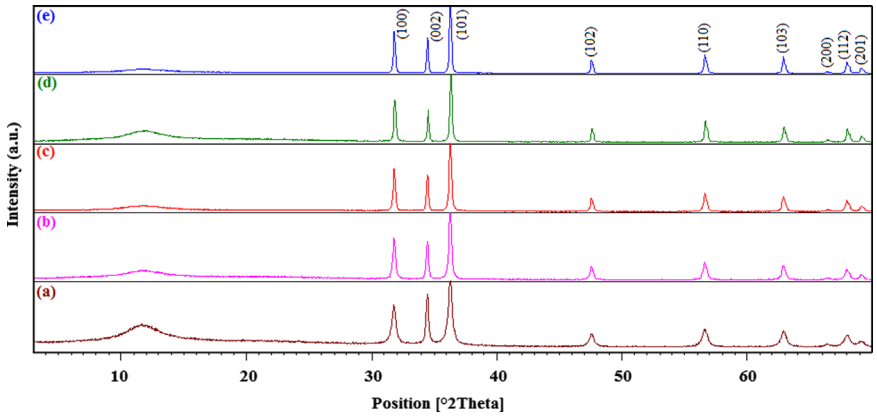


Fig. 1. XRD patterns of the mixture before hydrothermal treatment (a) and the as-synthesized samples at 180 °C for different reaction times: 0.5 h (b), 1 h (c), 3 h (d) and 24 h (e).

24 h, have been found to be, about 70 nm and 80 nm, respectively.

### 3.2. Morphology study

To understand the growth mechanism of the ZnO nanocrocrystals, an investigation was carried out on the morphology evolution of the samples with respect to different reaction times. Indeed, the morphology of synthesized samples was studied by using the scanning electron microscopy (SEM). Typical scanning electron microscopy images of the mixture before hydrothermal treatment and the samples synthesized at 180 °C for 0.5, 1, 3 and 24 h are shown in Fig. 2. It is clear that the morphology of the material synthesized for 24 h (Fig. 2e) is quite different from those synthesized for 0.5, 1, 3 h (Fig. 2b–d). It is possible to envisage that the reaction time has a profound effect on the particle size and the morphology. As shown in Fig. 2a, before hydrothermal treatment, only irregular particles structures were observed. In fact, the SEM reveals that the powder consists of heterogeneous particles. When the reaction time was prolonged to 0.5 h, only typical flower-like ZnO nanostructures consisted of the ZnO swords-like with 60–200 nm in width and several micrometers in length, as shown in Fig. 2b. Further increasing the reaction time to 1 h, a large amount of regular sword-like ZnO decorated by some particle began to form (Fig. 2c). When the reaction time is increased to 3 h, one can observe the existence of swords as well as pills-like (Fig. 2d). These swords particles are the intermediates for the formation of nanopills. After a 24 h synthesis process, the photo MEB shows a particle-made, homogeneous phase (Fig. 2e and f). It presents a rectangular, pill-like morphology with a hexagonal section of an average thickness of 50 nm (Fig. 2f). In fact, an increase in the reaction time brings about a change in the morphology of products.

It is well known that crystal formation in solution occurs in two steps: the first corresponds to occurrence of the crystal nucleation followed by crystal growth starting from the crystal nuclei. Consequently, the crystal nucleation growth rate is responsible for the formation of zinc oxide particles with

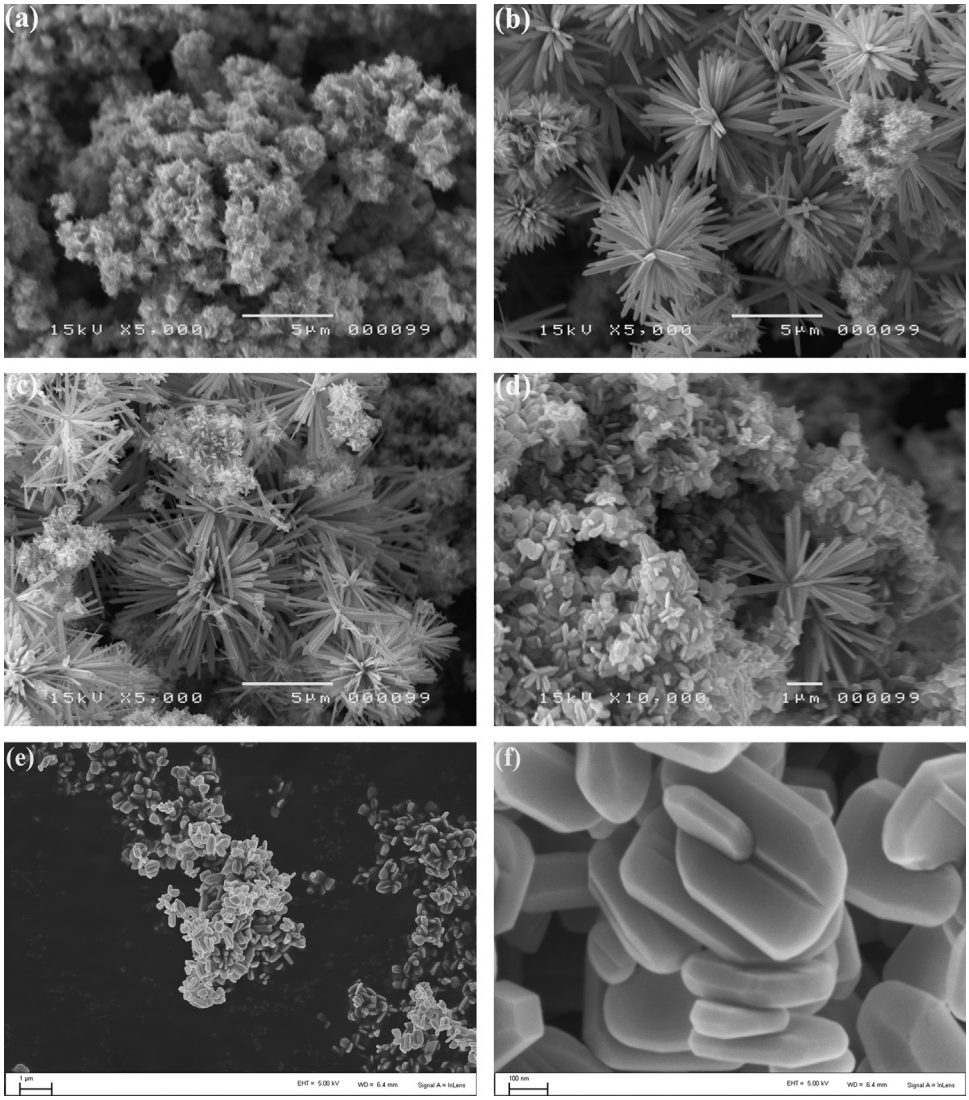


Fig. 2. SEM micrographs of the mixture before hydrothermal treatment (a) and the resulting products synthesized at 180 °C for different reaction times: 0.5 h (b), 1 h (c), 3 h (d), and 24 h (e, f).

different morphologies. In fact, the $Zn(OH)_2$ is more soluble than ZnO, the $Zn(OH)_2$ produces $Zn^{2+}$ and $OH^-$ ions, which form the ZnO nuclei [27]. ZnO behaves as polar crystal, where zinc and oxygen atoms are arranged alternatively along the *c*-axis and the top surface-plane is a Zn-terminated (001) plane while the bottom surface is oxygen-terminated $(00\bar{1})$ plane. The Zn-(001) is catalytically active while the O-$(00\bar{1})$ is inert [28]. Furthermore, the growth habit depends upon the growth velocities of different planes in the ZnO crystal.

### 3.3. Raman spectroscopy

Raman spectroscopy technique is very useful and sensitive for determining crystal perfection and structural defects. Fig. 3 shows the Raman scattering spectra of the as-synthesized ZnO nanoswords and nanopills. All samples showed similar Raman spectra. Hexagonal wurtzite ZnO belongs to the space group $C_{6v}^4(P_3^6mc)$ with two formula units in the primitive cell [29,30]. Group theory predicts the existence of the following optic modes: $A_1+2B_1+E_1+2E_2$, where, $A_1$, $E_1$ and $E_2$ are the first order Raman active modes and $B_1$ is forbidden [31]. As we can see in the spectra, a sharp, strong and dominant E2H mode of ZnO located at 437 $cm^{-1}$ is observed, which is the intrinsic characteristic of the Raman-active mode of wurtzite hexagonal ZnO [20]. Three very weak and suppressed peaks, at 330, 380 and 536 $cm^{-1}$ are also observed in the spectrum and assigned to the E2H–E2L (multi phonon), A1T and 2LA modes, respectively [32]. The appearance of a very suppressed and weak peak at 581 $cm^{-1}$ attributed to the E1L mode is also obtained. Generally, it is considered that the E1L mode is originated due to the formation of defects (oxygen vacancies or zinc interstitials) [33].

### 3.4. Infrared spectroscopy

The structure information was further provided by FTIR spectroscopy. It allows characterizing and evaluating the appearance and the disappearance of the chemical functions from the vibration modes of the liaisons of the molecules. Similar characteristics can be seen in the infrared spectra of the samples. Fig. 4 shows the infrared spectra of as-synthesized ZnO nanoswords (Fig. 4a) and nanopills (Fig. 4b). Indeed, the bands located at 3417 and 1619 $cm^{-1}$ are assigned to bending vibration and stretching vibration of O-H, originating from hydroxyl groups on the surface of the samples [34]. Therefore, the situated bands about 441 and 551 $cm^{-1}$ correspond, respectively, to the vibrations of elongation and of deformation of the vibratory zinc–oxygen in ZnO [35]. No typical absorption peak of organics can be found, proving that organic molecules are not strongly adsorbed on the ZnO crystal surface.

### 3.5. X-ray photoelectron spectroscopy (XPS)

The zinc valence state on the surface of the as-synthesized ZnO nanopills were further investigated by X-ray photoelectron spectroscopy (XPS), as shown in Fig. 5a the typical XPS survey spectrum of the as-synthesized ZnO. The XPS survey spectrum reveals that the sample only consists of zinc and oxygen (the C1s peak was appeared, which could be due to some $CO_2$ absorbed on the surface of the sample). All binding energies were corrected for the charge shift using the C1s peak of graphitic carbon (284 eV) as a reference [36]. From Fig. 5b, the Zn2p core-level of ZnO nanopills have two peaks located at about 1045 and 1021.98 eV attributed to $Zn2p_{1/2}$ and $Zn2p_{3/2}$, respectively. These results indicate that the chemical valence of Zn at the surface of ZnO nanopills is +2 oxidation state. However, The O1s region of ZnO nanopills can be fitted into three Gaussian peaks as shown in Fig. 5c. The first one, positioned at the lower binding energy of 530.27 eV, and is assigned to $O^{2-}$ ions in the Zn–O bonding of the wurtzite structure of ZnO [37]. The second peak located at 531.48 eV is assigned to OH group absorbed onto the surface of the ZnO nanoparticles [38]. The third, positioned at the higher binding energy of 532.52 eV can be ascribed to the presence of loosely bound oxygen on the surface of ZnO film such as, adsorbed $H_2O$ [39–41].

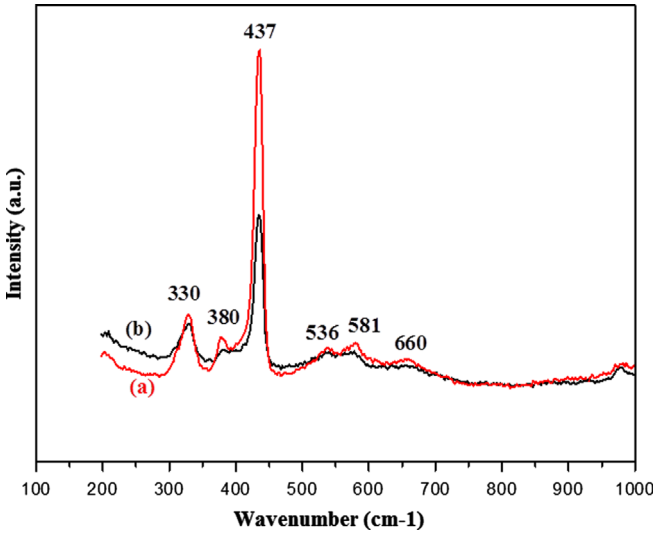


Fig. 3. Raman spectra of ZnO nanoswords (a) and nanopills (b).

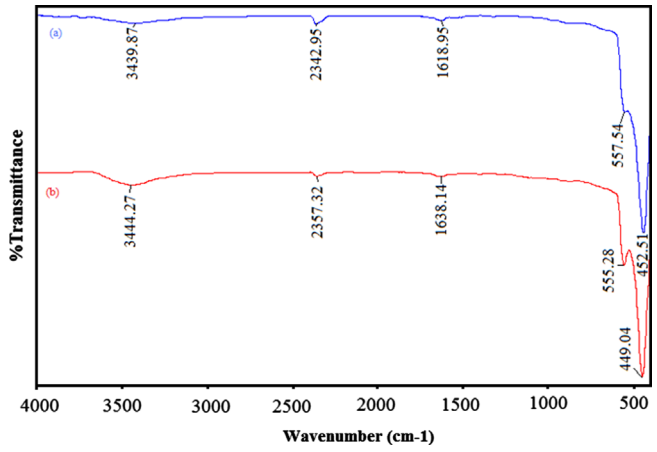


Fig. 4. FTIR spectra of ZnO nanoswords (a) and nanopills (b).

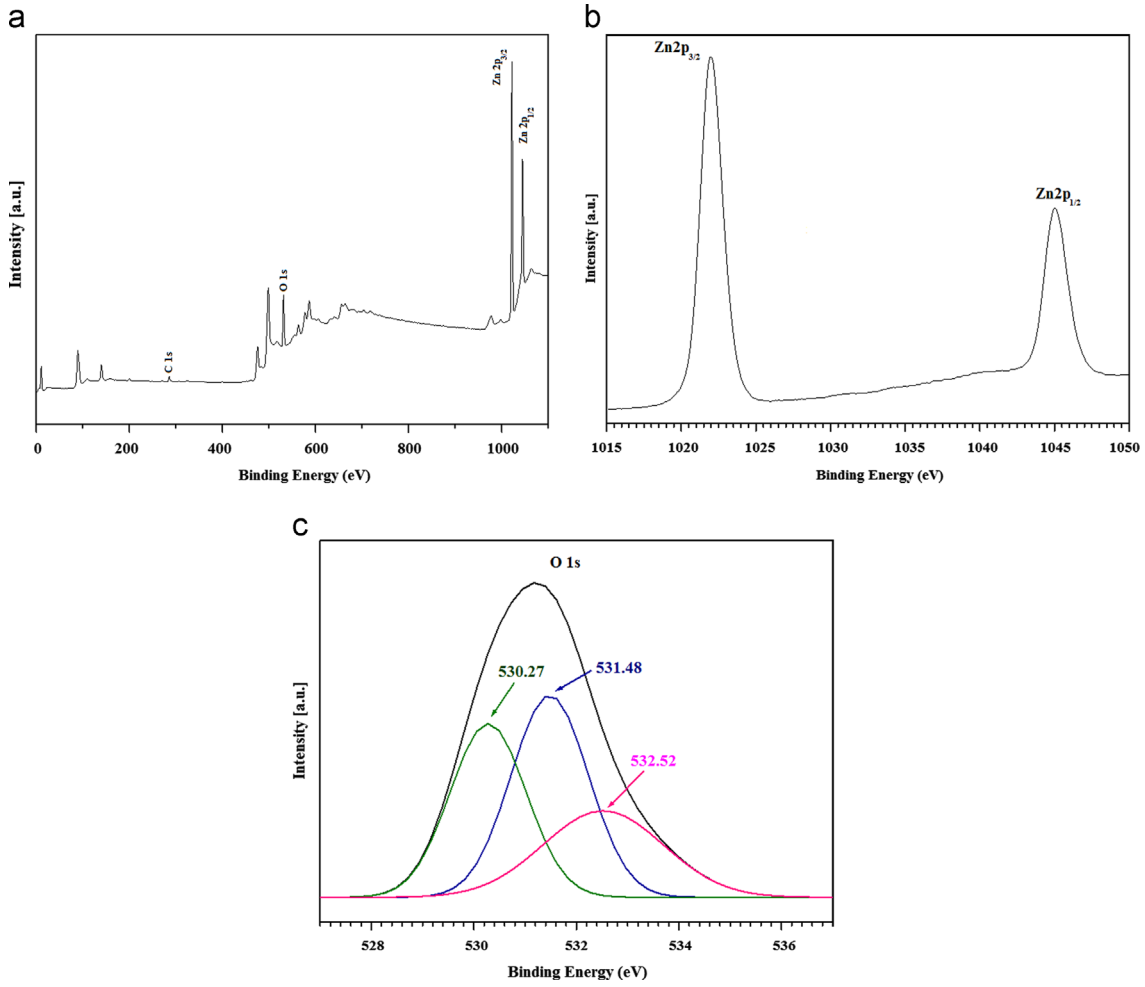


Fig. 5. The survey XPS spectrum of ZnO nanopills (a) and core level spectra of $Zn_{2p}$ (b), and $O_{1s}$ (c).

### 3.6. Optical properties

The optical properties of as-obtained ZnO were studied by UV–visible spectroscopy. The absorption spectra of the ZnO nanoswords and nanopills are shown in Fig. 6. In fact, the spectra exhibit an intense absorption below 400 nm to lower wavelengths. This is attributable to the intrinsic band gap absorption of ZnO at around 367 nm typically associated with a charge-transfer process from the valence band to conduction band. This is lower than the band gap wavelength of 388 nm for bulk ZnO [42]. Compared to the bulk ZnO, the observed change in ZnO nanoswords and nanopills may be due to the size effect [43,44]. Therefore, the interface and surface play a key role in the light absorption of the materials [45]. To make good use of the optical property difference between ZnO bulk and nanostructured, it is possible to apply the ZnO nanoswords and nanopills on the UV filter and photocatalysis.

The optical band gap, $E_g$, can be estimated from the following equation known as the Tauc plot [46]:

$$\alpha h\nu = (h\nu - E_g)^n$$

where $\alpha$ is the optical absorption coefficient, $h$ is the Planck constant, $\nu$ is the photon frequency, $E_g$ is optical band gap and

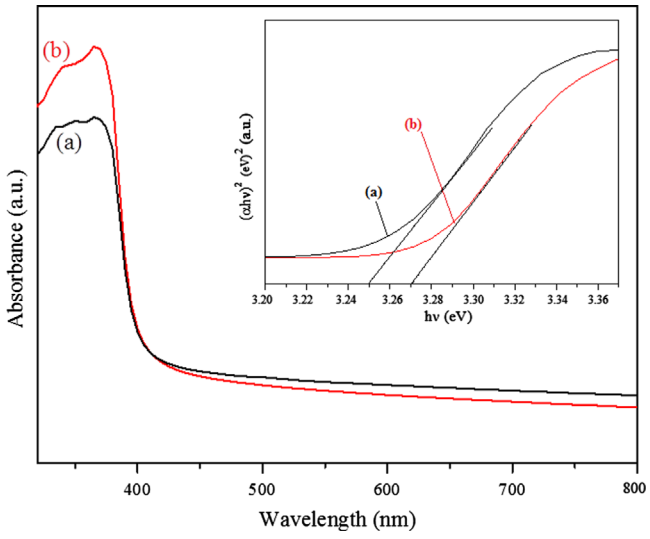


Fig. 6. UV–visible absorption spectra and the $(\alpha h\nu)^2$ versus $h\nu$ plot (inset) of ZnO nanoswords (a) and nanopills (b).

$n$ is a parameter associated with the type of electronic transition: $n=1/2$ for a direct allowed transition and $n=2$ for an indirect allowed transition. The inset in Fig. 6 presents the

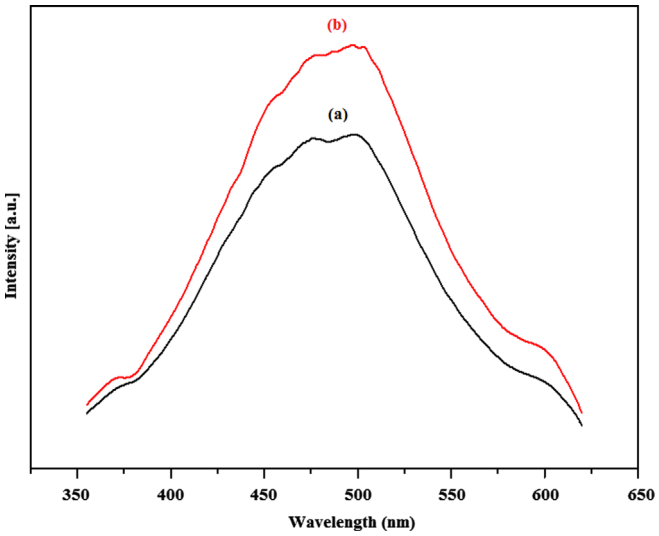


Fig. 7. Room temperature Photoluminescence spectra of ZnO nanoswords (a) and nanopills (b).

variation of $(\alpha h\nu)^2$ versus $h\nu$ for ZnO nanswords and nanopills. The optical band gap ($E_g$) can be calculated by extrapolating the linear portion of the plot of $(\alpha h\nu)^2$ versus $h\nu$ to $\alpha=0$. The values of $E_g$ for ZnO nanswords and nanopills are found to be 3.25 and 3.27 eV, respectively.

Photoluminescence (PL) spectra can explain the nature of the intrinsic defect in ZnO because the energy levels associate with the defects populating the large band gap of the material and producing radiative emissions at different wavelengths [47]. Room temperature PL properties of ZnO nanopills and nanoswords were also investigated. Fig. 7 shows the PL spectra of the ZnO nanopills and nanoswords under the excitation of the 325 nm Xe lamp. However, no obvious difference can be found in the emission spectra among ZnO products. The morphology changed from pill-like to sword-like only caused an increasing in the photoluminescent peak intensity; but the positions of the peaks hardly altered (Fig. 7). Previous research has shown that the PL spectra of ZnO are sensitive to the particles shape, size, and synthesis conditions [48,49]. In general, spectra are dominated by defect-related transitions, corresponding to vacancies and interstitial oxygen atoms [50]. Indeed, it is well known that there are various defects in ZnO, such as oxygen vacancies ($V_O$), zinc vacancies ($V_{Zn}$), interstitial oxygen ($O_i$), interstitial zinc ($Zn_i$), antisite oxygen ($O_{Zn}$) and so on [51]. The UV emission band at 376 nm in ZnO structure is also called near band edge (NBE) emission and is due to recombination of free-excitons (free excitations) via a process of exciton–exciton collisions [52]. Indeed, the low PL intensity at 376 nm indicates that the rate of the recombination between photogenerated holes and electrons might be lower on the surface of as-synthesized ZnO nanostructures than commercial ZnO powder, which is beneficial for the photocatalytic process [53]. A 453 nm blue emission peak in ZnO imply that electrons are trapped at interfaces lying within the depletion regions located at ZnO–ZnO grain boundaries [54]. The peak at 476 nm is related to Zn vacancy [55]. Moreover, the blue-green emission band centered at 497 nm is related to the exciton scattering by some definite defects, usually attributed to a singly charged oxygen vacancy or other defects, which originate from the recombination of a photoexcited hole with a charge state of the specific defect, such as oxygen vacancies, is also observed for both samples [31,54–56]. The green emission is generally related to a deep level or trap state emission. In fact, the deep level and trap state emission are assigned to the singly ionized oxygen vacancy and the irradiative recombination of a photo-generated hole with an electron occupying the oxygen vacancy, respectively [57]. The origin of the green-yellow emission located at 590 nm is attributed for more surface defects [58]. However, the yellow emission is attributed to the presence of oxygen vacancies in the crystal structure of ZnO [59].

## 4. Conclusion

Hexagonal zinc oxide nanoswords and nanopills were successfully synthesized via facile hydrothermal way by controlling the reaction conditions. It is believed that crystal nucleation and growth rates drastically affect the morphology of the obtained ZnO particles. XRD study demonstrated the existence of wrutzite ZnO of high degree of crystallinity with crystallite size in the range of 70–80 nm. In fact, the reaction time plays an important role in the formation process and can affect the shape and size of the ZnO crystal. The optical properties of the as-synthesized ZnO were investigated by UV–visible absorption and room temperature photoluminescence. Indeed, the values of the band gap $E_g$ for ZnO nanswords and nanopills are found to be 3.25 and 3.27 eV, respectively. The band gap obtained is higher than the bulk ZnO, which implies nanocrystalline nature of the material. The significant optical absorption properties of this material may be tempting for further application such as photocatalyst. This method, therefore, has high potentials to synthesize other nanocrystalline metal oxides.

## Acknowledgments

The authors thank Pr. A. Ghorbel (Laboratoire de Catalyse et Chimie des Matériaux, Faculté des Sciences de Tunis), Pr. M. Férid (Centre National des Recherches en Sciences des Matériaux, Technopole de Borj-Cedria) and H. Lecoq (ITO-DYS, Université Paris 7) for UV–vis, PL and MEB experiments.

## References

[1] Ü. Özgür, Ya.I. Alivov, C. Liu, A. Teke, M.A. Reshchikov, S. Doğan, V. Avrutin, S.J. Cho, H. Morkoç, A comprehensive review of ZnO materials and devices, Journal of Applied Physics 98 (2005) 041301.
[2] Q. Wu, X. Chen, P. Zhang, Y. Han, X. Chen, Y. Yan, S. Li, Amino acid-assisted synthesis of ZnO hierarchical architectures and their novel photocatalytic activities, Crystal Growth and Design 8 (2008) 3010–3018.
[3] J. Tian, Q. Zhang, L. Zhang, R. Gao, L. Shen, Sh. Zhang, X. Qu, G. Cao, ZnO/$TiO_2$nanocable structured photoelectrodes for CdS/CdSe quantum dot co-sensitized solar cells, Nanoscale 5 (2013) 936–943.

[4] D. Lee, W.K. Bae, I. Park, D.Y. Yoon, S. Lee, C. Lee, Transparent electrode with ZnO nanoparticles in tandem organic solar cells, Solar Energy Materials and Solar Cells 95 (2011) 365–368.
[5] Y. Li, B. Yao, R. Deng, B. Li, Z. Zhang, C. Shan, D. Zhao, D. Shen, A comparative studyon electroluminescence from ZnO-based double heterojunction light emitting diodesgrown on different lattice mismatch substrates, Journal of Alloys and Compounds 575 (2013) 233–238.
[6] Y. Zeng, T. Zhang, L. Wang, R. Wang, Synthesis and ethanol sensing properties of selfassembled monocrystalline ZnO nanorod bundles by poly (ethylene glycol)-assisted hydrothermal process, Journal of Physical Chemistry C 113 (2009) 3442–3448.
[7] W.E. Mahmoud, A.A. Al-Ghamdi, Synthesis of CdZnO thin film as a potential candidate for optical switches, Optics and Laser Technology 42 (2010) 1134–1138.
[8] Q. Xiang, G. Meng, Y. Zhang, J. Xu, P. Xu, Q. Pan, W. Yu, Ag nanoparticle embedded ZnO nanorods synthesized via a photochemical method and its gas-sensing properties, Sensors and Actuators B 143 (2010) 635–640.
[9] R.Y. Hong, J.H. Li, L.L. Chen, D.Q. Liu, H.Z. Li, Y. Zheng, J. Ding, Synthesis, surfacemodification and photocatalytic property of ZnO nanoparticles, Powder Technology 189 (2009) 426–432.
[10] A. Stanković, S. Dimitrijević, D. Uskoković, Influence of size scale and morphology onantibacterial properties of ZnO powders hydrothemally synthesized using different surface stabilizing agents, Colloids and Surfaces B 102 (2013) 21–28.
[11] R. Jalal, E.K. Goharshadi, M. Abareshia, M. Moosavi, A. Yousefi, P. Nancarrow, ZnOnanofluids: green synthesis, characterization, and antibacterial activity, Materials Chemistry and Physics 121 (2010) 198–201.
[12] A.L. Roest, J.J. Kelly, D. Vanmaekelbergh, E.A. Meulenkamp, Staircase in the electron mobility of a ZnO quantum dot assembly due to shell filling, Physical Review Letters 89 (2002) 036801.
[13] R. Mohan, K. Krishnamoorthy, S.J. Kim, Diameter dependent photocatalytic activity of ZnO nanowires grown by vapor transport technique, Chemical Physics Letters 539–540 (2012) 83–88.
[14] L.N. Protasova, E.V. Rebrov, K.L. Choy, S.Y. Pung, V. Engels, M. Cabaj, A.E.H. Wheatley, J.C. Schouten, ZnO based nanowires grown by chemical vapour deposition for selective hydrogenation of acetylene alcohols, Catalysis Science and Technology 1 (2011) 768–777.
[15] Y. Jouane, S. Colis, G. Schmerber, P. Kern, A. Dinia, T. Heiser, Y.-A. Chapuis, Room temperature ZnO growth by rf magnetron sputtering on top of photoactive P3HT: PCBM for organic solar cells, Journal of Materials Chemistry 21 (2011) 1953–1958.
[16] H.S. Desarkar, P. Kumbhakar, A.K. Mitra, One-step synthesis of Zn/ZnO hollow nanoparticles by the laser ablation in liquid technique, Laser Physics Letters 10 (2013) 055903.
[17] P. Kumbhakar, D. Singh, C.S. Tiwary, A.K. Mitra, Chemical synthesis and visible photoluminescence emission from monodispersed ZnO nanoparticles, Chalcogenide Letters 5 (2008) 389–396.
[18] S.K. Park, J.H. Park, K.Y. Ko, S. Yoon, K.S. Chu, W. Kim, Y.R. Do, Hydrothermal electrochemical synthesis of ZnO nanorods, Crystal Growth and Design 9 (2009) 3615–3620.
[19] K. Thongsuriwong, P. Amornpitoksuk, S. Suwanboon, The effect of aminoalcohols (MEA, DEA and TEA) on morphological control of nanocrystalline ZnO powders and its optical properties, Journal of Physics and Chemistry of Solids 71 (2010) 730–734.
[20] Y.F. Zhu, D.H. Fan, W.Z. Shen, Template-free synthesis of zinc oxide hollow microspheres in aqueous solution at low temperature, Journal of Physical Chemistry C 111 (2007) 18629–18635.
[21] A. Moulahi, F. Sediri, N. Gharbi, Hydrothermal synthesis of nanostructured zinc oxide and study of their optical properties, Materials Research Bulletin 47 (2012) 667–671.
[22] M. Chen, C.Y. Ma, T. Mahmud, J.A. Darr, X.Z. Wang, Modelling and simulation of continuous hydrothermal flow synthesis process for nanomaterials manufacture, Journal of Supercritical Fluids 59 (2011) 131–139.
[23] H. Zhang, D. Yang, Y. Ji, X. Ma, J. Xu, D. Que, Low temperature synthesis of flowerlike ZnO nanostructures by cetyltrimethylammonium bromide-assisted hydrothermal process, Journal of Physical Chemistry B 108 (2004) 3955–3958.
[24] J.H. Yang, J.H. Zheng, H.J. Zhai, L.L. Yang, L. Liu, M. Gao, Solvothermal growth of highly oriented wurtzite-structured ZnO nanotube arrays on zinc foil, Crystal Research and Technology 44 (2009) 619–623.
[25] T. Ghoshal, S. Kar, J. Ghatak, S. Chaudhuri, ZnO nanocones: solvothermal synthesis and photoluminescence properties, Materials Research Bulletin 43 (2008) 2228–2238.
[26] R. Huang, Y. Shen, L. Zhao, M. Yan, Effect of hydrothermal temperature on structure and photochromic properties of $WO_3$ powder, Advanced Powder Technology 23 (2012) 211–214.
[27] R. Wahab, S.G. Ansari, Y.S. Kim, H.K. Seo, G.S. Kim, G. Khang, H.S. Shin, Low temperature solution synthesis and characterization of ZnO nano-flowers, Materials Research Bulletin 42 (2007) 1640–1648.
[28] W.W. Lee, S.B. Kim, J. Yi, W.T. Nichols, W.I. Park, Surface polarity-dependent cathodoluminescence in hydrothermally grown ZnO hexagonal rods, Journal of Physical Chemistry C 116 (2012) 456–460.
[29] K.A. Salman, K. Omar, Z. Hassan, Effective conversion efficiency enhancement of solar cell using ZnO/PS antireflection coating layers, Solar Energy 86 (2012) 541–547.
[30] A. Sharma, B.P. Singh, S. Dhar, A. Gondorf, M. Spasova, Effect of surface groups on the luminescence property of ZnO nanoparticles synthesized by sol–gel route, Surface Science 606 (2012) L13–L17.
[31] M. Šćepanovic, M. Grujić-Brojčin, K. Vojisavljević, S. Bernik, T. Srećković, Raman study of structural disorder in ZnO nanopowders, Journal of Raman Spectroscopy 41 (2010) 914–921.
[32] S.K. Panda, C. Jacob, Surface enhanced Raman scattering and photoluminescence properties of catalytic grown ZnO nanostructures, Applied Physics A 96 (2009) 805–811.
[33] P. Jiang, J.J. Zhou, H.F. Fang, C.Y. Wang, Z.L. Wang, S.S. Xie, Hierarchical shelled ZnO structures made of bunched nanowire arrays, Advanced Functional Materials 17 (2007) 1303–1310.
[34] Q Yang, W. Hu, A novel mercury-media route to synthesize ZnO hollow microspheres, Ceramics International 36 (2010) 989–993.
[35] L. Wu, Y Wu, W. Lu, Preparation of ZnO nanorods and optical characterizations, Physica E 28 (2005) 76–82.
[36] R. Wahab, S.G. Ansari, H.-K. Seo, Y.S. Kim, E.-K. Suh, H.-S. Shin, Low temperature synthesis and characterization of rosette-like nanostructures of ZnO using solution process, Solid State Sciences 11 (2009) 439–443.
[37] J. Das, S.K. Pradhan, D.R. Sahu, D.K. Mishra, S.N. Sarangi, B.B. Nayak, S. Verma, B.K. Roul, Micro-Raman and XPS studies of pure ZnO ceramics, Physica B 405 (2010) 2492–2497.
[38] H. Zhou, Z. Li, Synthesis of nanowires, nanorods and nanoparticles of ZnO through modulating the ratio of water to methanol by using a mild and simple solution method, Materials Chemistry and Physics 89 (2005) 326–331.
[39] J. Lee, J. Chung, S. Lim, Improvement of optical properties of post-annealed ZnO nanorods, Physica E 42 (2010) 2143–2146.
[40] Jr-W. Peng, Po-C. Liu, S. Lee, Reversible band gap tuning of metal oxide films using hydrogen and oxygen plasmas, Thin Solid Films 531 (2013) 81–87.
[41] M. Chen, X. Wang, Y.H. Yu, Z.L. Pei, X.D. Bai, C. Sun, R.F. Huang, L.S. Wen, X-ray photoelectron spectroscopy and auger electron spectroscopy studies of Al-doped ZnO films, Applied Surface Science 158 (2000) 134–140.
[42] P. Kumbhakar, D. Singh, C.S. Tiwary, A.K. Mitra, Chemical synthesis and visible photoluminescence emission from monodispersed ZnO nanoparticles, Chalcogenide Letters 5 (2008) 387–394.
[43] X. Pu, D. Zhang, X. Yi, X. Shao, W. Li, M. Sun, L. Li, X. Qian, Rapid chemical synthesis and optical properties of ZnO ellipsoidal nanostructures, Advanced Powder Technology 21 (2010) 344–349.
[44] C. Wang, E. Shen, E. Wang, L. Gao, Z. Kang, C. Tian, Y. Land, C. Zhang, Controllable synthesis of ZnO nanocrystals via a surfactant-assisted alcohol thermal process at a low temperature, Materials Letters 59 (2005) 2867–2871.
[45] P.T. Hsieh, Y.C. Chen, K.S. Kao, M.S. Lee, C.C. Cheng, The ultraviolet emission mechanism of ZnO thin film fabricated by sol–gel technology, Journal of the European Ceramic Society 27 (2007) 3815–3818.

[46] J. Tauc, R. Grigorovici, A. Vancu, Optical properties and electronic structure of amorphous germanium, Physica Status Solidi B 15 (1966) 627–637.
[47] L. Wang, S.Z. Xu, H.J. Li, L.X. Chang, S. Zhi, M.H. Zeng, L.N. Wang, Y.N. Huang, Microbundles of zinc oxide nanorods: assembly in ionic liquid $[EMIM]^{+}[BF4]^{-}$, photoluminescence and photocatalytic properties, Journal of Solid State Chemistry 184 (2011) 720–724.
[48] Z.Q. Li, Y. Ding, Y.J. Xiong, Q. Yang, Y. Xie, Room-temperature surface-erosion route to ZnO nanorod arrays and urchin-like assemblies, Chemistry—A European Journal 10 (2004) 5823–5828.
[49] J.F. Coley, L. Stecker, Y. Ono, Directed assembly of ZnO nanowires on a Si substrate without a metal catalyst using a patterned ZnO seed layer, Nanotechnology 16 (2005) 292–296.
[50] M. Ali, M. Winterer, ZnO nanocrystals: surprisingly 'Alive', Chemistry of Materials 22 (2010) 85–91.
[51] A. Layek, B. Manna, A. Chowdhury, Carrier recombination dynamics through defect states of ZnO nanocrystals: from nanoparticles to nanorods, Chemical Physics Letters 539–540 (2012) 133–138.
[52] P.G Li, W.H. Tang, X. Wang, Synthesis of ZnO nanowire arrays and their photoluminescence property, Journal of Alloys and Compounds. 479 (2009) 634–637.
[53] J.H. Sun, S.Y. Dong, Y.K. Wang, S.P. Sun, Preparation and photocatalytic property of a novel dumbbell-shaped ZnO microcrystal photocatalyst, Journal of Hazardous Materials 172 (2009) 1520–1526.
[54] K.W. Wong, M.R. Field, J.Z. Ou, K. Latham, M.J. Spencer, I. Yarovsky, K. Kalantarzadeh, Interaction of hydrogen with ZnO nanopowders-evidence of hydroxyl group formation, Nanotechnology 23 (2012) 015705.
[55] C.F Windisch, G.J. Exarhos, C.H. Yao, L.Q. Wang, Raman study of the influence of hydrogen on defects in ZnO, Journal of Applied Physics 101 (2007) 123711–123717.
[56] C. Li, G Hong, P Wang, D Yu, L. Qi, Wet chemical approaches to patterned arrays of well-aligned ZnO nanopillars assisted by monolayer colloidal crystals, Chemistry of Materials 21 (2009) 891–897.
[57] K. Vanheusden, W.L. Warren, C.H. Seager, D.R. Tallant, J.A. Voigt, Mechanisms behind green photoluminescence in ZnO phosphor powders, Journal of Applied Physics 79 (1996) 7983–7990.
[58] K. Hou, Z. Gao, M. Da, Z. Li, H. Sun, J. Li, Y. Xie, T. Kang, A. Mijit, Oriented growth of urchin-like zinc oxide micro/nano-scale structures in aqueous solution, Materials Research Bulletin 47 (2012) 1010–1015.
[59] M.H. Huang, Y. Wu, H. Feik, N. Tran, E Weber, P. Yang, Catalytic growth of zinc oxide nanowires by vapor transport, Advanced Materials. 13 (2001) 113–116.